Author responses to review comments of "Sensitivity of airborne geophysical data to sublacustrine permafrost thaw" are detailed below.

B. Minsley
March 2015

L. Rabenstein
lasse.rabenstein@erdw.ethz.ch
Received and published: 12 January 2015

General comments

The paper examines the potential of AEM to detect the thawing stage of talik structures in sublacustrine permafrost. The study is working purely with 2D (?) synthetic data. The geophysical approach presented here is of high interest and importance for near-subsurface geophysical surveys and can be considered an example for hydrogeophysical studies in different environments. Studies, such as the presented one, can be used to enhance interpretation of AEM surveys over permafrost terrain. I would like to see this paper published in TC, but would appreciate if the following comments could be addressed:

I summarize the workings steps of the presented approach. If I made a mistake here, you could consider changing your text to a better understanding of this fact:

1. Obtainment of a realistic subsurface model for a talik structure. A previously developed hydrological algorithm (SUTRA) is used, to simulate a 1000 years of talik development, for a couple of different starting models with different lake levels and hydraulic gradients.
2. Derivation of electrical conductivity from the hydrological model parameters. An advanced form of Archies law was used. A variety of parameters are considered, as for instance temperature and ice-content.
3. For the derived electrical conductivity models (for various Talik evolution stages) 1D AEM forward calculations were done, in order to calculate synthetic AEM surveying data. Such data were calculated for subsurface models of every time step of the Talik evolution within the 1000 years.
4. A study to examine, how accurate the synthetic AEM data can be inverted to true subsurface conductivity models, using statistical approaches. Goal is to obtain likelihoods for parameters such as: number of layers, thickness of layers etc.

Response: Thank you for your comments. Your above summary of the general working steps of our approach are correct.

Reviewer comment:

The Abstract and Introduction should more prominently state, that this paper describes a study with synthetic data ONLY. 2D or 3D?

Response:
The Abstract and Introduction already contain five references to 'synthetic' or 'simulated' results- two additional instances are described below, and we also added reference to the two-dimensional axis-symmetric modeling domain. We also clarify that the hydrologic model has a two-dimensional axis-symmetric geometry- while simulations are fundamentally 2D (radial distance & depth), they represent 3D physics under the assumption of radial symmetry.

Changes:
Two sentences modified in the Abstract: "Several *numerical modeling* scenarios are evaluated that consider the response to variable hydrologic forcing from different lake depths and hydrologic gradients", and "A final *synthetic* example compares AEM and ground-based electromagnetic responses for their ability to resolve shallow permafrost and thaw features in the upper 1-2 m below ground."

Introduction, last paragraph: "The coupled thermal-hydrologic simulations of Wellman et al. (2013) predict the evolution of lake taliks (unfrozen sub-lacustrine areas in permafrost regions) *in a two-dimensional axis-symmetric model* under different environmental scenarios (e.g. lake size, climate, groundwater flow regime).

Reviewer comment:
I understand, that the study examines the ability of AEM to detect not only Talik structures in general, but to detect different stages of a 1000 years of Talik evolution. If this is correct, please state this more clearly already in the Abstract and Introduction. However, I doubt, that in reality you can assign an inverted AEM resistivity model to a stage of a 1000 years of Talik evolution. You rather will obtain a general idea of where thawed areas are situated.

Response: We do not mean to suggest that we can assign any particular resistivity interpretation to a specific stage of talik evolution over the 1000 year simulation time. We do, however, demonstrate that general subsurface thaw conditions can be identified, and that this can give insight into whether talik formation at a particular location might be relatively new or if it has been established for some time. While geophysical data represent just one snapshot in time, a comparison across different lakes in one area may be able to identify relatively new versus older taliks.

Changes:
Added to end of 1st paragraph in Section 2.4: "*AEM-derived resistivity estimates for the simulations considered here will help guide interpretations of future field datasets, identifying the characteristics of relatively young versus established thaw under different hydrologic conditions.*"

Reviewer comment:

Can you explain in the text how the variance of 100'000 different resistivity models is created by the McMC appoach? Changing starting models? Changed inversion parameters?

Response:
McMC algorithms are well documented in the literature, and we did not want to distract from the talik simulation study to review the McMC method. A Markov chain is a mathematical framework for drawing samples from the model-space posterior distribution. Each of the 100,000 samples is drawn sequentially (starting from an arbitrary point in model-space) according to the Metropolis-Hastings algorithm (cited in the paper). In contrast with traditional inversion methods that find a single 'best' model given some starting model and inversion parameters, the McMC approach samples many (100,000 in our case) models consistent with the data in order to quantify model uncertainty.

Reviewer comment:
Please specify which kind of inversion the McMC approach uses. I understand that also the McMC study needs a "normal" inversion algorithm?

Response:
McMC is, itself, an alternate to "normal" inversion approaches. Instead of being an optimization algorithm that finds a single 'best' model that fits data (plus any model regularization), McMC is a sampling method that estimates the true posterior distribution of model parameters.

Changes:
Added to the 1st paragraph of section 2.4: "*This McMC approach is an alternative to traditional inversion methods that find a single 'optimal' model that minimizes a combined measure of data fit and model regularization (Aster et al., 2005). Although computationally more demanding, McMC methods allow for comprehensive model appraisal and uncertainty quantification.*"

Reviewer comment:
How large is the noise added to the synthetic data?

Changes:
Modified 2nd sentence in Section 3.2: "The simulated data are then used to recover estimates of the original resistivity values according to the approach outlined in Section 2.4*, assuming 4% data error with an absolute error floor of 5 ppm.*"

Modified last paragraph of section 3.3: "*An error model with 4% relative data errors and an absolute error floor of 75 ppm was used for the GEM-2 data."*

Reviewer comment:
I would appreciate if the study addresses, how accurate the resistivity models would be, without the McMC method, just simple inversion with one result and one RMS value, as this is the standard you are going to improve.

Response:
McMC does not necessarily lead to a more accurate result, but rather a comprehensive assessment of model uncertainty. We recognize that any single model derived from a simple inversion can be misleading as choices of inversion algorithm and parameters can lead to many different results that fit the data equally well. By using the McMC approach we aim to be as transparent as possible with regards to linking possible geophysical models to true simulations. This is discussed in Section 2.4 (including new changes described earlier).

Reviewer comment:
I would appreciate, if the novelty in this approach is more clearly stated. For me as a reader it was not entirely clear, whether the novelty was in the combination of several other studies to a new approach or the application of other approaches in a series, or whether there was a significantly new calculation step involved?

Response:
There are several aspects in which this work is novel, building on existing studies: (1) Our incorporation of a surface conduction term in the electrical property model that facilitates modeling of changes both as a function of ice content and lithology, (2) coupling geophysical predictions to process-based hydrologic simulations is not new, but has not previously been done for simulations of permafrost impacted hydrologic systems, and (3) uncertainty quantification of AEM findings and their implications for permafrost interpretations.

Changes:
Modified in Abstract: "*A novel* physical property relationship connects the dynamic distribution of electrical resistivity to ice-saturation and temperature outputs from the SUTRA groundwater simulator with freeze/thaw physics."

Modified in Conclusions: "Coupled hydrogeophysical simulations using a *novel* physical property relationship that accounts for the effects of lithology, ice saturation, and temperature on electrical resistivity provide a systematic framework for exploring the geophysical response to various scenarios of permafrost evolution under different hydrological forcing... A robust uncertainty analysis of the geophysical simulations provides *important new* quantitative information about the types of features that can be resolved using AEM data given the inherent resolution limitations of geophysical measurements and ambiguities in the physical property relationships"

Specific comments

Reviewer comment:
I needed quite some time to extract important information about the study from the text (synthetic only, AEM study for a lot of stages throughout the 1000 years, . . .). I made suggestions to improve the text towards a quicker understanding of these facts. In italic are text passages from the paper, normal font are comments from my side, and in red text suggestions, where I think more stringent and exact writing could improve the understanding and clearness of the text.

Abstract Page 6080: Sorry for being pedantic but the abstract is the most important section of a paper, and I would like to understand it, without reading the entire paper:

Several scenarios are evaluated that consider the response (of what???) *to variable hydrologic forcing from* (better at?) *different lake depths and* for different *hydrologic gradients*.

Changes:
Several numerical modeling scenarios are evaluated that consider the *non-isothermal hydrologic* response to variable forcing from different lake depths and *for different* hydrologic gradients.

Reviewer comment:
The model includes a physical property relationship that connects the dynamic distribution of subsurface electrical resistivity based on lithology as well as ice-saturation and temperature outputs from the SUTRA groundwater simulator with freeze/thaw physics.
Can you break it into two sentences? It took me quite some time to get the meaning of the sentence . . . After I have read the entire paper, the sentence was easy to understand, but anyway, in the Abstract it should be easy to understand without any prior knowledge about the study.

Changes:
Modified abstract: "A *novel* physical property relationship connects the dynamic distribution of electrical resistivity *to* ice-saturation and temperature outputs from the SUTRA groundwater simulator with freeze/thaw physics. T*he influence of lithology on electrical resistivity is controlled by a surface conduction term in the physical property relationship.*"

Reviewer comment:
Electrical resistivity models are used to simulate AEM data in order to explore the sensitivity of geophysical observations to permafrost thaw. It is clear that you need

electrical resistivity models as an input to simulate AEM data. Can you state more specifically what is special about the resistivity models? Something like a range of resistivity models, which reflect the progressing permafrost thaw, are used as an input to calculate synthetic AEM data in order to . . .

Changes:
Modified abstract: "*R*esistivity models*, which reflect changes in subsurface conditions,* are used *as inputs* to simulate AEM data in order to explore the sensitivity of geophysical observations to permafrost thaw."

Reviewer comment:
Synthetic geophysical data (Too general, what kind of data, the AEM data?) *are analyzed with a Bayesian Markov chain Monte Carlo algorithm that provides a probabilistic assessment of geophysical model uncertainty* (too general, what kind of model?) *and resolution*.

Changes:
Modified abstract: "Synthetic *AEM* data are analyzed with a Bayesian Markov chain Monte Carlo algorithm that quantifies geophysical *parameter* uncertainty and resolution."

Reviewer comment
Major lithological and permafrost features are well resolved (by the resistivity model inverted from the AEM data?) *in the examples considered*.

Changes:
Modified abstract: "Major lithological and permafrost features are well resolved *by AEM data* in the examples considered."

Reviewer comment:
A final example compares AEM and ground-based (on a lake? Maybe the title sublacustrine is not entirely correct?) *electromagnetic responses for their ability to resolve shallow permafrost* (still sublacustrine? .. After I have read the paper it was clear that this ground study was done for the regions outside the lake, however, then the title is not covering this part of the study) *and thaw features in the upper 1–2 m below ground.*

Changes:
Modified abstract: "A final synthetic example compares AEM and ground-based electromagnetic responses for their ability to resolve shallow permafrost and thaw features in the upper 1-2 m below ground *outside the lake margin*."

Modified title: "Sensitivity of airborne geophysical data to sublacustrine *and near-surface* permafrost thaw"

Reviewer comment:
Introduction: Page 6082
. . .expected for various permafrost hydrologic conditions occurring within the 1000 years of simulated Talik formation.

Changes:
Modified last paragraph of Introduction: "This is accomplished in three steps: … (2) *generation* of synthetic geophysical data that would be expected for various permafrost hydrologic conditions *that occur during simulated lake talik formation*; and …."

Reviewer comment:
Methods: 2.1. Is the model 2D or 3D? How is ice content calculated? I would appreciate a sentence or two describing the major factor responsible for thaw in the simulation?

Response:
We state in Section 2.1 that the model is axis-symmetric- so technically it is 2D, but accounts for the 3D geometry of flow surrounding a circular lake. Regarding ice content and simulating thaw, Wellman et al. (2013) state: "The US Geological Survey (USGS) SUTRA code (Voss and Provost 2002), which simulates unsaturated flow, groundwater (saturated) flow, and heat or solute transport, was extended to incorporate the phase change between ice and liquid water by McKenzie et al. (2007). The enhanced code simulates dynamic ice formation when subsurface temperatures fall below a specified maximum freezing temperature. Ice saturation, defined as the fraction of ice in the total pore volume, varies over a specified temperature range from 0 (thus, liquid saturation=1) at the maximum freezing temperature, to 1 minus a specified residual liquid saturation at the minimum freezing temperature. As ice forms or thaws, the code accounts for latent heat of fusion, changes in thermal conductivity and heat capacity for mixtures of liquid water and ice in the pore space, and changes in the effective permeability of the porous medium as impacted by ice content." The primary driver of thaw is the transition from terrestrial initial conditions to a lake system with greater average temperatures and reduced seasonal amplitude beneath the newly formed lake.

Changes:
Added to Section 2.1: "*The phase change between ice and liquid water occurs over a specified temperature range, and accounts for latent heat of fusion, as well as changes in thermal conductivity and heat capacity for ice-water mixtures. Ice content also changes the effective permeability, thereby altering subsurface flowpaths and enforcing a strong coupling between hydraulic and thermal processes*"

Reviewer comment:
2.2. The theory seems to be well described and cited with literature. I could not see any major flaw on the theory how it is introduced, but must admit, that I am not an expert in the presented Theory. It might be good when a dedicated expert to electrical conductivity material relations is having a look on chapter 2.2.

Response:
Thank you for your comment- this section is mainly an adaptation of the theory presented by co-author Revil in his cited 2012 work.

Reviewer comment:
Page 6081: *However, few techniques are capable of assessing the distribution of permafrost, and most approaches only capture a single snapshot in time.* Are you talking about geophysical surveying techniques? In a 1000 years evolution, isn't every geophysical survey just a single snapshot in time?

Response:
This was a generic comment meant to refer to any sort of hydrologic/geophysical/remote sensing observation. While most observations represent a single snapshot in time, there are also examples of time-lapse surveys or data logging (though of course none of these would be relevant to a 1000 year time period).

Reviewer comment:
... physical properties (e.g. electrical resistivity) are only *indirectly sensitive to physical...*

Changes:
Modified sentence in Introduction: "A challenge with geophysical methods, however, is that geophysical properties (e.g. electrical resistivity) are *only* indirectly sensitive to physical properties of interest (e.g. lithology, water content, thermal state)."

Reviewer comment:
Chapter 2.2.
. . . associated magnetic fields created by *the transmitter coils induce electrical currents in the*

Changes:
Modified sentence in Section 2.3: "Oscillating currents and associated magnetic fields *created by* the transmitter coils induce electrical currents in the subsurface that, in turn,

generate secondary magnetic fields that are recorded by the receiver coils (Siemon, 2006; Ward and Hohmann, 1988)."

Reviewer comment:
Data are simulated at the nominal survey elevation of 30m above ground surface using the one-dimensional modeling equations described in Minsley (2011). Please explain what is special about the equations in Minsley (2011), or add something like . . . which follow the standard theory given in e.g. Ward and Hohmann (1988)

Response:
The specific algorithm used for modeling was developed in Minsley (2011), though this follows the theory of Ward and Hohmann (1988) as you mention.

Changes:
Modified last sentence in first paragraph of section 2.3: "Data are simulated at the nominal survey elevation of 30 m above ground surface using the one-dimensional modeling *algorithm* described in Minsley (2011)*, which follows the standard electromagnetic theory presented by Ward and Hohmann (1988)*."

Reviewer comment
2.4.:
resistivity values throughout the 1000 year lake talik simulations. . . . resistivity values for various (or yearly, what was the time resolution of the SUTRA model?) stages throughout the 1000 years of Talik evolution?

Response:
SUTRA models have a <1 year time resolution, but here we worked with outputs at 20 year intervals.

Changes:
Modified 1st paragraph of Section 2.4: "Here, we use a Bayesian Markov chain Monte Carlo (McMC) algorithm developed for frequency-domain EM data (Minsley, 2011) to explore the ability of simulated AEM data to recover the true distribution of subsurface resistivity values *at 20-year intervals within* the 1,000-year lake talik simulations.

Reviewer comment:
an ensemble of 100 000 resistivity models is inverted from the same synthetic AEM data set (did I understand this correctly?) *,according to the Metropolis–Hastings algorithm (Hastings, 1970; Metropolis et al., 1953).*

Changes:

Modified sentence in 2nd paragraph of section 2.4: "At every data location along the survey profile, an ensemble of 100,000 resistivity models is *generated* according to the Metropolis-Hastings algorithm (Hastings, 1970; Metropolis et al., 1953)."

Reviewer comment:
3.2.:
Geophysical data (not shown) are simulated AEM data? Please specifiy.

Changes:
Modified 1st sentence of section 3.2: "*AEM* data (not shown) are simulated for each of the electrical resistivity models (e.g. Figure 4) using the methods described in Section 2.3."

Reviewer comment:
Discussion Page 6095:
Understanding the hydrogeophysical responses to permafrost . . . You mean the AEM responses? Please specify.

Response:
I meant this comment to be broader than just AEM responses. It is really the coupled hydrologic and geophysical response we are interested in (hence the term hydrogeophysical).

Reviewer comment:
. . . coupling geophysical predictions . . . Please specify geophysical

... analysis of geophysical uncertainty ... Please specify geophysical

Changes:
Modified sentence in Discussion: "We have presented a general framework for coupling *airborne and ground-based electromagnetic* predictions to hydrologic simulations of permafrost evolution, including a novel physical property relationship that accounts for the electrical response to changes in lithology, temperature, and ice content, as well as a rigorous analysis of geophysical *parameter* uncertainty."

Reviewer comment:
as well as thermally and hydrologically induced changes in permafrost over time (Figs. 8 and 9). Are you talking about the 1000 years period? Can you dicuss how resistivity changes over 1000 years is of practical use in real surveys? . . . Okay,later in the discussion chapter you address this issue. But the sentence confuses at this position in the text.

Changes:
Modified sentence in Discussion: "In the specific examples of lake talik evolution presented here, which are modeled after the physical setting of the Yukon Flats, Alaska (Minsley et al., 2012b), AEM data are shown to be generally capable of resolving large-scale permafrost and geological features (Figure 5), as well as thermally and hydrologically induced changes in permafrost (Figure 8, Figure 9)." [*deleted phrase 'over time'].*

Reviewer comment:
The Bayesian McMC analysis provides useful details about model resolution and uncertainty that cannot be assessed using traditional inversion methods that produce a single "best" model. I would appreciate a discussion about how wrong you are, when using traditional inversion, without McMC. Isn't traditional inversion also a part of the McMC analysis? See General comments as well.

Response:
See earlier response to general comment. McMC does not necessarily lead to a more accurate result compared with traditional inversion, but it does provide substantial information about parameter uncertainty that is typically not contained in traditional inversion results. In a traditional inversion, incorporation of a specific model regularization makes the inverse problem unique and solvable, but does not convey the degree to which other models are also consistent with the data (and should also be considered).

Reviewer response:
Summary:
. . . associated with the co-evolution of permafrost and hydrologic systems. . . The evolution happens over hundreds of years, how is AEM useful here. Are you saying, that the presented model study allows to assign inverted AEM resistivity models to a stage of permafrost evolution?

Response:
Correct, we do not suggest that geophysics would be useful in monitoring change over this timescale. But the resistivity data do provide insight as to the stage of permafrost evolution at a particular location.

Reviewer response:
Table 1: How is the difference between Unit 1 and 2 characterized? Both have the same porosity. Okay, at the end of chapter 2.2. you tell it is differentiated by Xi. You could make this clearer in Table 1 and earlier in the text. I understand Xi to be the major controlling quantity and should be highlighted more prominent.

Response:
Correct, the difference in unit 1 and 2 is their cation exchange capacity. These values are noted in the 2nd to last row of table 2. We also state in Section 2.2, "Changes in χ, representative of bulk differences in clay mineral content, are used to differentiate the electrical signatures of the lithologic units in this study (Table 1)."

Reviewer comment:
Figure 10c. Can you comment on the deeper high conductivity artifact at app. r=750 m? How is this possible with synthetic data?

Response:
The data are synthetic, but have also had realistic noise added to them. This specific location probably represents a situation where incorrect model structure was fit to the noisy data.

Anonymous Referee #2
Received and published: 2 February 2015

Reviewer Comments :
This paper demonstrates the ability of airborne geophysical techniques (AEM) to characterize subsurface physical properties associated with talik formation beneath lakes. The results of this work can help to improve techniques to both identify and delineate taliks beneath lakes and also to monitor their evolution over time. This is important for development of ground water models which are required for example, for planning mining developments and the assessment of their environmental effects. Identification of hydraulic connections between mining project components such as open pit/underground mines and tailing impoundments and surrounding water bodies is a key consideration in planning mining projects.

The paper is appropriate for publication in The Cryosphere. A few comments, from a permafrost perspective, are offered for the authors' consideration.

Methods, Section 2.1 Additional information would be useful regarding the initial study conditions such as the initial ground temperature conditions and permafrost thickness.

Response*:* Initial permafrost conditions are detailed in Wellman et al. [2013]: "The permafrost structure that existed prior to the appearance of the lake was obtained by running the model to steady state under hydrostatic conditions with a constant temperature of −2.25 °C applied to the land surface. The applied surface temperature, thermal properties, and geothermal heat flux produces a laterally continuous permafrost layer extending to a depth of about 90 m. This is the initial

condition, representing the system in a state prior to lake formation"

Changes: Added sentence to end of 1st paragraph in Section 2.1, "*Initial permafrost conditions prior to lake formation were established by running the model to steady state under hydrostatic conditions with a constant temperature of –2.25 °C applied to the land surface, which produces a laterally continuous permafrost layer extending to a depth of about 90 m.*"

Reviewer Comment:
Results/Discussion For fine-grained sediments such as silt and clay, a significant amount of unfrozen water may exist below 0◦C. The unfrozen water content curve (unfrozen water vs temperature) for fine-grained material therefore differs from that for coarser grained sands and gravels. Perhaps the authors could add a bit more about the range in temperatures for which the unfrozen water content may make it difficult to determine talik boundaries. For warm permafrost conditions where temperatures are close to 0◦C one could delineate a talik from the AEM survey (due to lower resistivity) in finer grained material which is larger than that which would be defined based on only temperature (i.e. permafrost at temperatures below 0◦C).

Response: We agree that the amount of unfrozen water, which differs as a function of temperature in different types of sediments, can complicate the interpretation of talik presence/absence. In part this is complicated by the term 'talik', which does not account for the warm permafrost conditions near 0◦C that you describe. The distinction between using resistivity data to infer the presence of a talik based on unfrozen water content versus temperature is an important one to consider.

Changes: Added to end of 3rd paragraph in Section 4 (Discussion), "*Finally, it is important to note that resistivity is sensitive primarily to unfrozen water content, and that significant unfrozen water can remain in relatively warm permafrost that is near 0 C, particularly in fine-grained sediments. Resistivity-derived estimates of talik boundaries defined by water content may therefore differ from the thermal boundary defined at 0 C.*"

Reviewer Comment:
The authors mention (page 6097) that AEM data are most likely to be useful for baseline characterization of subsurface properties as opposed to monitoring changes in permafrost. Perhaps the authors could comment more on the effectiveness of delineating through taliks which is a key consideration in the identification of hydraulic connections between water bodies. What are the limitations of the technique regarding permafrost conditions as presumably the technique would not be as useful for identification of through taliks under colder conditions where permafrost is thicker.

Response: Difficulty in delineating fully through-going thaw conditions compared with partial thaw is discussed in detail in the Discussion section. We also discuss the fortuitous nature of the Yukon Flats geology upon which this study was based, where the gravel/silt resistivity contrast helps to identify when fully-thawed conditions exist. The challenge in identifying through-going conditions would be exacerbated in thicker permafrost conditions due to the decreasing resolution of AEM data with depth.

Changes: Modified 2nd paragraph in Discussion section, "If the order of these layers were reversed, if the base of permafrost were hosted in a relatively resistive lithology, *or if the base of permafrost was significantly deeper*, AEM data would not likely resolve the overall structure with such good fidelity."

Reviewer Comment:
I would agree with the authors that for the most part under natural conditions, changes in permafrost occur over a longer time period than is practical for repeat AEM surveys. However there are situations related to human activity where repeat surveys might be practical. One situation where use of AEM as a monitoring tool might be considered is where lakes are formed behind dams. This would be the case for water supply reservoirs and for mine tailing impoundments. Over several years a talik will form as there is a significant change in ground surface temperature conditions (rapid change from a mean ground surface temperature of several degrees below 0◦C to temperatures above 0◦C). There may also be situations either natural or related to human activity where (rapid) lake drainage may occur resulting in freezing of taliks beneath the former lakes and it is not clear whether AEM might be useful for monitoring these changes.

Response: We agree that there could be some value for AEM related to baseline characterization and monitoring impacts related to large-scale infrastructure projects that could cause permafrost change over short timeframes.

Changes: Added sentence to last paragraph of Discussion section, "*One exception could be related to infrastructure projects such as water reservoirs or mine tailing impoundments behind dams, where AEM could be useful for baseline characterization and repeat monitoring of the impact caused by human-induced permafrost change.*"

Sensitivity of airborne geophysical data to sublacustrine and near-surface permafrost thaw

Burke J. Minsley[1], Tristan P. Wellman[2], Michelle A. Walvoord[3], and André Revil[4,5]

[1] {U.S. Geological Survey, Crustal Geophysics and Geochemistry Science Center, Denver, Colorado}

[2] {U.S. Geological Survey, Colorado Water Science Center, Denver, Colorado}

[3] {U.S. Geological Survey, National Research Program, Denver, Colorado}

[4] {Colorado School of Mines, Department of Geophysics, Golden, Colorado}

[5] {JSTerre, CNRS, UMR CNRS 5275, Université de Savoie, Le Bourget du Lac, France}

Abstract

A coupled hydrogeophysical forward and inverse modeling approach is developed to illustrate the ability of frequency-domain airborne electromagnetic (AEM) data to characterize subsurface physical properties associated with sublacustrine permafrost thaw during lake talik formation. Numerical modeling scenarios are evaluated that consider non-isothermal hydrologic responses to variable forcing from different lake depths and for different hydrologic gradients. A novel physical property relationship connects the dynamic distribution of electrical resistivity to ice-saturation and temperature outputs from the SUTRA groundwater simulator with freeze/thaw physics. The influence of lithology on electrical resistivity is controlled by a surface conduction term in the physical property relationship. Resistivity models, which reflect changes in subsurface conditions, are used as inputs to simulate AEM data in order to explore the sensitivity of geophysical observations to permafrost thaw. Simulations of sublacustrine talik formation over a 1,000-year period are modeled after conditions found in the Yukon Flats, Alaska. Synthetic AEM data are analyzed with a Bayesian Markov chain Monte Carlo algorithm that quantifies geophysical parameter uncertainty and resolution. Major lithological and permafrost features are well resolved by AEM data in the examples considered. The subtle geometry of partial ice-saturation beneath lakes during talik formation cannot be resolved using AEM data, but the gross characteristics of sub-lake resistivity models reflect bulk changes in ice content and can identify the presence of a talik. A final synthetic example compares AEM and ground-based electromagnetic responses for their ability to resolve shallow permafrost and thaw features in the upper 1-2 m below ground outside the lake margin.

Burke Minsley 3/2/2015 3:15 PM
Deleted: Several

Burke Minsley 2/23/2015 11:50 PM
Deleted: the

Burke Minsley 2/23/2015 10:55 PM
Deleted: hydrologic

Burke Minsley 2/23/2015 11:26 PM
Deleted: The model includes a

Burke Minsley 2/23/2015 11:26 PM
Deleted: that

Burke Minsley 2/23/2015 11:50 PM
Deleted: subsurface

Burke Minsley 2/23/2015 11:31 PM
Deleted: based on lithology as well as

Burke Minsley 2/23/2015 11:45 PM
Deleted: Electrical r

Burke Minsley 2/23/2015 11:36 PM
Deleted: , are evaluated

Burke Minsley 2/24/2015 7:38 AM
Deleted: geophysical

Burke Minsley 2/23/2015 11:43 PM
Deleted: provides a probabilistic assessment of

Burke Minsley 2/24/2015 7:43 AM
Deleted: model

Burke Minsley 2/23/2015 11:55 PM
Deleted: be used to determine

1 Introduction

Permafrost thaw can have important consequences for the distribution of surface water (Roach et al., 2011; Rover et al., 2012), stream discharge and chemistry (O'Donnell et al., 2012; Petrone et al., 2007; Striegl et al., 2005; Walvoord and Striegl, 2007), and exchange between groundwater and surface water systems (Bense et al., 2009; Callegary et al., 2013; Walvoord et al., 2012). Likewise, hydrologic changes that alter the thermal forcing supplied by surface water or groundwater systems can modify the distribution of permafrost, illustrating the strong feedbacks between permafrost and hydrology. In addition to hydrologic processes, permafrost is affected by climate warming in Arctic and sub-Arctic regions (Hinzman et al., 2005; Jorgenson et al., 2001), as well as disturbance by fire (Yoshikawa et al., 2002). Climate feedbacks associated with permafrost thaw include changes in the amount of organic carbon stored in soils that is vulnerable to decomposition (Koven et al., 2011; O'Donnell et al., 2011) and subsequent methane and carbon dioxide released from soils by the degradation of organic material previously sequestered in frozen ground (Anthony et al., 2012). Permafrost thaw also has significant implications for land management and infrastructure, including the potential to damage buildings, roadways, or pipelines due to ground settling, and thermal erosion that can alter coastlines and landscape stability (Larsen et al., 2008; Nelson et al., 2002).

Several investigations have shown the significance of climate and advective heat transport in controlling the distribution of permafrost in hydrologic systems (Bense et al., 2009; Rowland et al., 2011; Wellman et al., 2013). These results yield important insight into the mechanistic behavior of coupled thermal-hydrologic systems, and are a means for predicting the impact on permafrost from a wide range of climate and hydrologic conditions. However, few techniques are capable of assessing the distribution of permafrost, and most approaches only capture a single snapshot in time.

Satellite remote-sensing techniques have proven useful in detecting the distribution and changes in shallow permafrost, vegetation, and active layer thickness over large areas (Liu et al., 2012; Panda et al., 2010; Pastick et al., 2014), but are only sensitive to very near-surface properties. Borehole cores and downhole temperature or geophysical logs provide direct information about permafrost and geologic structures, but tend to be

sparsely located and are not always feasible in remote areas. Geophysical methods are necessary for investigating subsurface physical properties over large and/or remote areas. Recent examples of geophysical surveys aimed at characterizing permafrost in Alaska include: an airborne electromagnetic (AEM) survey used to delineate geologic and permafrost distributions in an area of discontinuous permafrost (Minsley et al., 2012a), ground-based electrical measurements used to assess shallow permafrost aggradation near recently receded lakes (Briggs et al., 2014), electrical and electromagnetic surveys used to characterize shallow active layer thickness and subsurface salinity (Hubbard et al., 2013), and surface nuclear magnetic resonance (sNMR) soundings used to infer the thickness of unfrozen sediments beneath lakes (Parsekian et al., 2013). A challenge with geophysical methods, however, is that geophysical properties (e.g. electrical resistivity) are only indirectly sensitive to physical properties of interest (e.g. lithology, water content, thermal state). In addition, various physical properties can produce similar electrical resistivity values. Therefore, it is critically important to understand the relationship between geophysical properties and the ultimate physical properties and processes of interest (Minsley et al., 2011; Rinaldi et al., 2011).

The non-isothermal hydrologic simulations of Wellman et al. (2013) predict the evolution of lake taliks (unfrozen sub-lacustrine areas in permafrost regions) in a two-dimensional axis-symmetric model under different environmental scenarios (e.g. lake size, climate, groundwater flow regime). Here, we investigate the ability of geophysical measurements to recover information about the underlying spatial distribution of permafrost and hydrologic properties. This is accomplished in three steps: (1) development of a physical property relation that connects permafrost and hydrologic properties to geophysical properties; (2) generation of synthetic geophysical data that would be expected for various permafrost hydrologic conditions that occur during simulated lake talik formation; and (3) inversion of the synthetic geophysical data using realistic levels of noise to investigate the ability to resolve specific physical features of interest. Our focus is on electromagnetic geophysical methods as these types of data have previously been acquired near Twelvemile Lake in the Yukon Flats, Alaska (Ball et al., 2011; Minsley et al., 2012a); a lake that is also the basis for the lake simulations discussed by Wellman et al. (2013).

Burke Minsley 2/24/2015 8:08 AM
Deleted: coupled thermal-

Burke Minsley 2/24/2015 9:21 PM
Deleted: simulation

2 Methods

2.1 Coupled Thermal-hydrologic Simulations

Wellman et al. (2013) describe numerical simulations of lake-talik formation in watersheds modeled after those found in the lake-rich Yukon Flats of interior Alaska. Modeling experiments used the SUTRA groundwater modeling code (Voss and Provost, 2002) enhanced with capabilities to simulate freeze-thaw processes (McKenzie and Voss, 2013). The phase change between ice and liquid water occurs over a specified temperature range, and accounts for latent heat of fusion as well as changes in thermal conductivity and heat capacity for ice-water mixtures. Ice content also changes the effective permeability, thereby altering subsurface flowpaths and enforcing a strong coupling between hydraulic and thermal processes. The modeling domain, which is adapted for this study, is axis-symmetric with a central lake and upwards-sloping ground surface that rises from an elevation of 500 m at $r = 0$ m to 520 m at the outer extent of the model, $r = 1800$ m (Figure **1**). The model uses a layered-geology consistent with the Yukon Flats (Minsley et al., 2012a; Williams, 1962), with defined hydrologic and geophysical parameters for each layer summarized in Table **1**. Initial permafrost conditions prior to lake formation were established by running the model to steady state under hydrostatic conditions with a constant temperature of −2.25 °C applied to the land surface, which produces a laterally continuous permafrost layer extending to a depth of about 90 m.

Subsequent hydrologic simulations assume fully saturated conditions, and are performed over a 1,000-year period under 36 different scenarios of climate (warmer than, colder than, and similar-to present conditions); hydrologic gradient (hydrostatic, gaining, and losing lake conditions); and lake depth/extent (3- , 6- , 9- , and 12-m-deep lakes that intersect the ground surface at increasing distance, as shown in Figure **1**). Complete details and results of the hydrologic simulations can be found in Wellman et al. (2013). At each simulation time step, the SUTRA model outputs temperature, pressure, and ice saturation. Conversion of these hydrologic variables to electrical resistivity- the geophysical property needed to simulate electromagnetic data considered here- is described below.

Burke Minsley 2/21/2015 1:10 PM
Deleted: Hydrologic

2.2 A physical property relationship

Electrical resistivity is the primary geophysical property of interest for the electromagnetic geophysical methods used in this study. It is well-established that resistivity is sensitive to basic physical properties such as unfrozen water content, soil or rock texture, and salinity (Palacky, 1987). Here, we build on earlier efforts to simulate the electrical properties of ice-saturated media (Hauck et al., 2011) by using a modified form of Archie's Law (Archie, 1942) that also incorporates surface conduction effects (Revil, 2012) to predict the dynamic electrical resistivity structure for the evolving state of temperature and ice saturation (S_i) in the talik simulations. Bulk electrical conductivity is described by *Revil* (2012) as

$$\sigma = \frac{S_w^n}{F}\left[\sigma_f + m\left(S_w^{-n}F - 1\right)\sigma_s\right], \quad (1)$$

where σ is the bulk electrical conductivity [S/m]; S_w is the fractional water saturation [-] in the pore space, where $S_w = 1 - S_i$; σ_f is the conductivity of the saturating pore fluid [S/m]; m is the Archie cementation exponent [-]; n is the Archie saturation exponent [-]; F is the formation factor [-], where $F = \phi^{-m}$ and ϕ is the matrix porosity [-]; and σ_s is the conductivity [S/m] associated with grain surfaces. The Archie exponents m and n are known to vary as a function of pore geometry; here, we use $m = n = 1.5$, which is appropriate for unconsolidated sediments (Sen et al., 1981). Simulation results are presented as electrical resistivity [ohm-m], which is the inverse of the conductivity, i.e. $\rho = 1/\sigma$.

The first term in Eq. (1) describes electrical conduction within the pore fluid, where fluid conductivity is defined as

$$\sigma_f = F_c \sum_i \beta_i |z_i| C_i \ . \quad (2)$$

The summation in Eq. (2) is over all dissolved ionic species (Na^+ and Cl^- are assumed to be the primary constituents in this study), where F_c is Faraday's constant [C/mol] and C_i, β_i, and z_i are the concentration [mol/L], ionic mobility [m^2/Vs], and valence of the i^{th} species, respectively.

800 Surface conduction effects, described by the second term in Eq. (1), are related to the
801 chemistry at the pore-water interface, and can be important in fresh water (low
802 conductivity) systems at low porosity (high ice saturation). Additionally, the surface
803 conduction term provides a means for describing the conductivity behavior for different
804 lithologies, as will be described below. The surface conductivity is given by

805 $$\sigma_s = \frac{2}{3}\left(\frac{\phi}{1-\phi}\right)\beta_s Q_v \,, \tag{3}$$

806 where β_s is the cation mobility [m^2/Vs] for counterions in the electrical double layer at the
807 grain-water interface (Revil et al., 1998) and Q_v is the excess electrical charge density
808 [C/m^3] in the pore volume,

809 $$Q_v = S_w^{-1}\rho_g\left(\frac{1-\phi}{\phi}\right)\chi \,, \tag{4}$$

810 where ρ_g is the mass density of the grains [kg/m^3] and χ is the cation exchange capacity
811 [C/kg]. Changes in χ, representative of bulk differences in clay mineral content, are used
812 to differentiate the electrical signatures of the lithologic units in this study (Table **1**).

813 The temperature, T [C], dependence of ionic mobility affects both the fluid conductivity
814 (Eq. (2)) and surface conductivity (Eq. (3)), where mobility is approximated as a linear
815 function of temperature (Keller and Frischknecht, 1966; Sen and Goode, 1992) as

816 $$\beta(T) = \beta_{T=25\mathrm{C}}\left[1 + 0.019(T-25)\right]. \tag{5}$$

817 Finally, we consider the effect of increasing ice saturation on salinity. Because salts are
818 generally excluded as freezing occurs, salinity of the remaining unfrozen pore water is
819 expected to increase with increasing ice content (Marion, 1995), leading to a
820 corresponding increase in fluid conductivity according to Eq. (2). To describe this
821 dependence of salinity on ice saturation, $C(S_i)$, we use the expression

822 $$C(S_i) = C_{S_i=0}S_w^{-\alpha}, \tag{6}$$

823 where $\alpha \sim 0.8$ accounts for loss of solute from the pore space due to diffusion or other
824 transport processes, and $S_i = 1 - S_w$.

Information about the different lithologic units described by Wellman et al. (2013) that are also summarized in Table **1** are used to define static model properties such as porosity, grain mass density, cation exchange capacity, and Archie's exponents. Dynamic outputs from the SUTRA simulations, including temperature and ice saturation, are combined with the static variables in Eqs. (1) - (6) to predict the evolving electrical resistivity structure.

2.3 Geophysical Forward Simulations

Synthetic airborne electromagnetic (AEM) data are simulated for each snapshot of predicted bulk resistivity values using nominal system parameters based on the Fugro RESOLVE[1] frequency-domain AEM system that was used in the Yukon Flats survey (Minsley et al., 2012a). The RESOLVE system consists of five horizontal coplanar (HCP) transmitter-receiver coil pairs separated by approximately 7.9 m that operate at frequencies 0.378 kHz, 1.843 kHz, 8.180 kHz, 40.650 kHz, and 128.510 kHz; and one vertical coaxial (VCX) coil pair with 9-m separation that operates at 3.260 kHz. Oscillating currents and associated magnetic fields created by the transmitter coils induce electrical currents in the subsurface that, in turn, generate secondary magnetic fields that are recorded by the receiver coils (Siemon, 2006; Ward and Hohmann, 1988). Data are reported as in-phase and quadrature components of the secondary field in parts-per-million (ppm) of the primary field, and responses as a function of frequency can be converted through mathematical inversion to estimates of electrical resistivity as a function of depth (e.g., Farquharson et al., 2003). Data are simulated at the nominal survey elevation of 30 m above ground surface using the one-dimensional modeling algorithm described in Minsley (2011), which follows the standard electromagnetic theory presented by Ward and Hohmann (1988).

The vertical profile of resistivity as a function of depth is extracted at each survey location and is used to simulate forward geophysical responses. There are 181 sounding locations for each axis-symmetric model, starting at the center of the lake (r = 0 m) to the edge of the model domain (r = 1,800 m) in 10-m increments. Each vertical resistivity

[1] Any use of trade, product, or firm names is for descriptive purposes only and does not imply endorsement by the U.S. Government

Burke Minsley 2/25/2015 8:51 AM
Formatted: Font:(Default) +Theme Body

Burke Minsley 2/24/2015 9:52 PM
Deleted: in the

Burke Minsley 2/24/2015 9:57 PM
Deleted: equations

profile extends to 200 m depth, which is well beyond the depth to which we expect to recover parameters in the geophysical inversion step. A center-weighted 5-point filter with weights equal to [0.0625, 0.25, 0.375, 0.25, 0.0625] is used to average neighboring bulk resistivity values at each depth before modeling in order to partly account for the lateral sensitivity of AEM systems (Beamish, 2003). Forward simulations are repeated for each of the 50 simulation times between 0 and 1,000 years output from SUTRA, resulting in 9,050 data locations per modeling scenario.

Synthetic ground-based electromagnetic data presented in Section 3.3 are simulated using nominal system parameters based on the GEM-2 instrument (Huang and Won, 2003). The GEM-2 has a single HCP transmitter-receiver pair separated by 1.66 m, and data are simulated at six frequencies: 1.5 kHz, 3.5 kHz, 8.1 kHz, 19 kHz, 43 kHz, and 100 kHz. A system elevation of 1 m above ground is assumed, which is typical for this hand-carried instrument.

2.4 Parameter Estimation and Uncertainty Quantification

The inverse problem involves estimating subsurface resistivity values given the simulated forward responses and realistic assumptions about data errors. Geophysical inversion is inherently uncertain; there are many plausible resistivity models that are consistent with the measured data. In addition, the ability to resolve true resistivity values is limited both by the physics of the AEM method and the level of noise in the data. Here, we use a Bayesian Markov chain Monte Carlo (McMC) algorithm developed for frequency-domain EM data (Minsley, 2011) to explore the ability of simulated AEM data to recover the true distribution of subsurface resistivity values at 20-year intervals within the 1,000-year lake talik simulations. This McMC approach is an alternative to traditional inversion methods that find a single 'optimal' model that minimizes a combined measure of data fit and model regularization (Aster et al., 2005). Although computationally more demanding, McMC methods allow for comprehensive model appraisal and uncertainty quantification. AEM-derived resistivity estimates for the simulations considered here will help guide interpretations of future field datasets, identifying the characteristics of relatively young versus established thaw under different hydrologic conditions.

Burke Minsley 2/24/2015 10:03 PM
Deleted: throughout

Burke Minsley 2/23/2015 8:27 PM
Deleted:

The McMC algorithm provides comprehensive model assessment and uncertainty analysis, and is useful in diagnosing the ability to resolve various features of interest. At every data location along the survey profile, an ensemble of 100,000 resistivity models is generated according to the Metropolis-Hastings algorithm (Hastings, 1970; Metropolis et al., 1953). According to Bayes' theorem, each model is assigned a posterior probability that is a measure of (1) its prior probability which, in this case, is used to penalize models with unrealistically large contrasts in resistivity over thin layers; and (2) its data likelihood, which is a measure of how well the predicted data for a given resistivity model match the observed data within data errors. A unique aspect of this algorithm is that it does not presuppose the number of layers needed to fit the observed data, which helps avoid biases due to assumptions about model parameterization. Instead, trans-dimensional sampling rules (Green, 1995; Sambridge et al., 2013) are used to allow the number of unknown layers to be one of the unknowns. That is, the unknown parameters for each model include the number of layers, layer interface depths, and resistivity values for each layer.

Burke Minsley 2/23/2015 8:59 PM
Deleted: sampled

Numerous measures and statistics are generated from the ensemble of plausible resistivity models, such as: the single most-probable model, the probability distribution of resistivity values at any depth, the probability distribution of where layer interfaces occur as a function of depth, and the probability distribution of the number of layers (model complexity) needed to fit the measured data. A detailed description of the McMC algorithm can be found in Minsley (2011). Finally, probability distributions of resistivity are combined with assumptions about the distribution of resistivity values for any lithology and/or ice content in order to make a probabilistic assessment of lithology or ice content, as illustrated below.

3 Results

3.1 Electrical resistivity model development

Information about the different lithologic units described by Wellman et al. (2013) that are also summarized in Table **1** are used to define static model properties such as porosity, grain mass density, cation exchange capacity, and Archie's exponents. Dynamic outputs from the SUTRA simulations, including temperature and ice saturation,

are combined with the static variables in Eqs. (1) - (6) to predict the evolving electrical resistivity structure. The behavior of bulk resistivity as a function of ice saturation is shown in Figure **2**. Separate curves are shown for a range of χ (cation exchange capacity) values, which are the primary control in defining offset resistivity curves for different lithologies, where increasing χ is generally associated with more fine-grained material such as silt or clay.

For each of the 1,000-year simulations, the static variables summarized in Table **1** are combined with the spatially and temporally variable state variables T and S_i output by SUTRA to predict the distribution of bulk resistivity at each time step using Eqs. (1) - (6). An example of SUTRA output variables for the 6 m-deep gaining lake scenario at 240 years (the approximate sub-lake talik breakthrough time for that scenario) is shown in Figure **3**A-B, and the predicted resistivity for this simulation step is shown in Figure **3**C. The influence of different lithologic units is clearly manifested in the predicted resistivity values, whereas lithology is not overly evident in the SUTRA state variables. For a single unit, there is a clear difference in resistivity for frozen versus unfrozen conditions. Across different units, there is a contrast in resistivity when both units are frozen or unfrozen. Resistivity can therefore be a valuable indicator of both geologic and ice content variability. However, there is also ambiguity in resistivity values as both unfrozen Unit 2 and frozen Unit 3 appear to have intermediate resistivity values of approximately 100-300 ohm-m (Figure **3**C) and cannot be characterized by their resistivity values alone. This ambiguity in resistivity can only be overcome by additional information such as borehole data or prior knowledge of geologic structure. Synthetic bulk resistivity values according to Eq. (1) are shown in Figure **4** for the four different lake depths (3, 6, 9, and 12 m) at three different simulation times (100, 240, and 1,000 years) output from the hydrostatic/current climate condition simulations.

Lithology and ice saturation are the primary factors that control simulated resistivity values (Figure **2**), though ice saturation is a function of temperature. The empirical relation between temperature and bulk resistivity is shown in Figure **3**D by cross-plotting values from Figure **3**B-C. Within each lithology resistivity is relatively constant above zero degrees, with a rapid increase in resistivity for temperatures below zero degrees. This result is very similar to the temperature-resistivity relationships illustrated by

Hoekstra (1975, Fig. 1), lending confidence to our physical property definitions described earlier. Above zero degrees, the slight decrease in resistivity is due to the temperature-dependence of fluid resistivity. The rapid increase in resistivity below zero degrees is primarily caused by reductions in effective porosity due to increasing ice saturation, though changes in surface conductivity and salinity at increasing ice saturation are also contributing factors. Below -1C, the change in resistivity values as a function of temperature rapidly decreases. This is an artifact caused by the imposed temperature-ice saturation relationship defined in SUTRA that, for these examples, enforces 99% ice saturation at -1C. It is more likely that ice saturation continues to increase asymptotically over a larger range of temperatures below zero degrees, with corresponding increases in electrical resistivity. However, because AEM methods are limited in their ability to discern differences among very high resistivity values, as discussed later, this artifact does not significantly impact the results presented here.

3.2 Parameter Estimation and Uncertainty Quantification

AEM data (not shown) are simulated for each of the electrical resistivity models (e.g. Figure **4**) using the methods described in Section 2.3. The simulated data are then used to recover estimates of the original resistivity values according to the approach outlined in Section 2.4, assuming 4% data error with an absolute error floor of 5 ppm. Resistivity parameter estimation results for the 6 m-deep hydrostatic lake scenario (Figure **4**, D-F) are shown in Figure **5**. At each location along the profile, the average resistivity model as a function of depth is calculated from the McMC ensemble of 100,000 plausible models. The overall pattern of different lithologic units and frozen/unfrozen regions is accurately depicted in Figure **5**, with two exceptions that will be discussed in greater detail: (1) the specific distribution of partial ice saturation beneath the lake before thaw has equilibrated (Figure **5**A-B); and (2) the shallow sand layer (Unit 1) that is generally too thin to be resolved using AEM data.

A point-by-point comparison of true (Figure **4**F) versus predicted (Figure **5**C) resistivity values for the hydrostatic 6 m-deep lake scenario at the simulation time 1,000 years is shown in Figure **6**A. The cross-plot of true versus estimated resistivity values generally fall along the 1:1 line, providing a more quantitative indication of the ability to estimate

Burke Minsley 2/24/2015 10:09 PM
Deleted: Geophysical

the subsurface resistivity structure. Estimates of the true resistivity values for each lithology and freeze/thaw state (Figure **6**B) tend to be indistinct; appearing as a vertical range of possible values in Figure **6**A due to the inherent resolution limitations of inverse methods and parameter tradeoffs (Day-Lewis, F. D. et al., 2005; Oldenborger and Routh, 2009). Although the greatest point density for both frozen and unfrozen silts (Unit 3) falls along the 1:1 line, resistivity values for these components of the model are also often overestimated; this is likely due to uncertainties in the location of the interface between the silt and gravel units. This is in contrast with the systematic underestimation of frozen gravel resistivity values due to the inability to discriminate very high resistivity values using EM methods (Ward and Hohmann, 1988). Frozen sands (true log resistivity ~2.8 in Figure **6**B) are also systematically overestimated in Figure **6**A; in this case, due to the inability to resolve this relatively thin resistive layer.

Unknown
Field Code Changed

While useful, single 'best' estimates of resistivity values at any location (Figure **6**) are not fully representative of the information contained in the AEM data and associated model uncertainty. From the McMC analysis of 100,000 models at each data location, estimates of the posterior probability density function (pdf) of resistivity are generated for each point in the model. Probability distributions are extracted from a depth of 15 m, within the gravel layer (Unit 2), at one location where unfrozen conditions exist (r = 0 m), and a second location outside the lake extent (r = 750 m) where the ground remains frozen (Figure **7**A**)**. Results from a depth of 50 m, within the silt layer (Unit 3), are shown in Figure **7**B. With the exception of the frozen gravels, whose resistivity tends to be underestimated, the peak of each pdf is a good estimate of the true resistivity value at that location.

Resistivity values are translated to estimates of ice saturation, which is displayed on the upper axis of each panel in Figure **7**, using the appropriate lithology curve from Figure **2**. Using the ice saturation-transformed pdfs, quantitative inferences can be made about the probability of the presence or absence of permafrost. For example, the probability of ice content being less than 50% is estimated by calculating the fractional area under each distribution for ice-content values less than 0.5. Probability estimates of ice content less than 50% and greater than 95% for the four distributions shown in Figure **7** are summarized in Table **2**. High probabilities of ice content exceeding 95% are associated

1010 with the r = 750 m location outside the lake extent, whereas high probability of ice
1011 content below the 50% threshold are observed at r = 0 beneath the center of the lake. The
1012 pdfs for each lithology shown in Figure **7** are end-member examples of frozen and
1013 unfrozen conditions. Within a given lithology, a smooth transition from the frozen-state
1014 pdf to the unfrozen-state pdf is observed as thaw occurs, with corresponding transitions in
1015 the calculated ice threshold probabilities.

1016 Further illustration of the spatial and temporal changes in resistivity pdfs are shown in
1017 Figure **8**. The resistivity pdf is displayed as a function of distance from the lake center at
1018 the same depths (15 m and 50 m) shown in Figure **7**, corresponding to gravel (Figure
1019 **8**A,C, and E) and silt (Figure **8**B, D, and F) locations. High probabilities, i.e. the peaks in
1020 Figure **7**, correspond to dark-shaded areas in Figure **8**. Images are shown for three
1021 different time steps in the SUTRA simulation for the hydrostatic 6 m-deep lake scenario:
1022 100 years (Figure **8**A-B), 240 years (Figure **8**C-D), and 1,000 years (Figure **8**E-F).
1023 Approximate ice-saturation values, translated from the ice versus resistivity relationships
1024 for each lithology shown in Figure **2**, are displayed on the right axis of each panel in
1025 Figure **8**, and true resistivity values are plotted as a dashed line. Observations from
1026 Figure **8** include:

1027 (1) Outside the lake boundary, pdfs are significantly more sharply peaked (darker
1028 shading) for the gravel unit than the silt unit, suggesting better resolution of shallower
1029 resistivity values within the gravel layer. It should be noted however, that this improved
1030 resolution does not imply improved model accuracy; in fact, the highest probability
1031 region slightly underestimates the true resistivity value. (2) Probability distributions for
1032 the silt layer track the true values, but with greater uncertainty. (3) Inside the lake
1033 boundary, gravel resistivity values are not as well resolved compared with locations
1034 outside the lake boundary due to the loss of signal associated with the relatively
1035 conductive lake water. (4) Increasing trends in resistivity/ice saturation towards the outer
1036 extents of the lake are captured in the pdfs, but are subtle. (5) Within the silt layer at
1037 early times before the talik is fully through-going (Figure **8**B, D), the AEM data are
1038 insensitive to which layer is present, hence the bi-modal resistivity distribution with
1039 peaks associated with characteristic silt and gravel values. This ambiguity disappears at

later times when the low-resistivity unfrozen silt layer extends to the base of the unfrozen gravels, which is a more resolvable target (Figure **8**F).

A more detailed analysis of the changes in resistivity and ice-saturation as a function of time, and for the differences between hydrostatic and gaining lake conditions, is presented in Figure **9**. Average values of resistivity/ice-saturation within 100 m of the lake center are shown within the gravel layer at a depth of 15 m (Figure **9**A) and a depth of 50 m within the silt layer (Figure **9**B) at 20 year time intervals. Outputs are displayed for both 6 m-deep hydrostatic and gaining lake scenarios. Thawing due to conduction occurs over the first ~200 years within the gravel layer (Figure **9**A), with similar trends for both the hydrostatic and gaining lake conditions and no clear relationship to the talik formation times indicated as vertical lines. Conduction-dominated thaw is observed for the gravel layer in the gaining lake scenario because significant advection does not occur until after the thaw bulb has extended beneath the gravel layer. In the deeper silt layer (Figure **9**B), however, very different trends are observed for the hydrostatic and gaining lake conditions. Ice content decreases gradually as thawing occurs in the hydrostatic scenario, consistent with conduction-dominated thaw, reaching a minimum near the time of talik formation at 687 years (Wellman et al., 2013, Table 3). In contrast, there is a rapid loss in ice content in the gaining lake scenario resulting from the influence of advective heat transport as groundwater is able to move upwards through the evolving talik beneath the lake. This rapid loss in ice content begins after the gravel layer thaws, and reaches a minimum near the 258-year time of talik formation for this scenario. These trends, captured by the AEM-derived resistivity models, are consistent with the plots of change in ice volume output from the SUTRA simulations reported by Wellman et al. (2013, Figure 3).

3.3 Near-Surface Resolution

Finally, we focus on the upper sand layer (Unit 1), which is generally too thin (2 m) and resistive (> 600 ohm-m) to be resolved using AEM data; though may be imaged using other ground-based electrical or electromagnetic geophysical methods. Seasonal thaw and surface runoff causes locally reduced resistivity values in the upper 1 m, which is still too shallow to resolve adequately using AEM data. In practice, shallow thaw and sporadic permafrost trends are observed to greater depths in many locations, including

inactive or abandoned channels (Jepsen et al., 2013b). To simulate these types of features, the shallow resistivity structure of the 6 m-deep hydrostatic lake scenario at 1,000 years is manually modified to include three synthetic 'channels'. These channels are not intended to represent realistic pathways relative to the lake and the hydrologic simulations; they are solely for the purpose of illustrating the ability to resolve shallow resistivity features.

Figure **10**A shows the three channels in a zoomed-in view of the uppermost portion of the model outside the lake extent. Each channel is 100 m wide, but with different depths: 1 m (half the Unit 1 thickness), 2 m (full Unit 1 thickness) and 3 m (extending into the top of Unit 2). Analysis of AEM data simulated for this model, presented as the McMC average model, are shown in Figure **10**B. All three channels are clearly identified, but their thicknesses and resistivity values are overestimated and cannot be distinguished from one another. To explore the possibility of better resolving these shallow features, synthetic EM data are simulated using the characteristics of a ground-based multi-frequency EM tool (the GEM-2 instrument) that can be hand carried or towed behind a vehicle, and is commonly used for shallow investigations. The McMC average model result for the simulated shallow EM data is shown in Figure **10**C. An error model with 4% relative data errors and an absolute error floor of 75 ppm was used for the GEM-2 data. Channel thicknesses and resistivity values are better resolved compared with the AEM result, though the 1 m-deep channel near r = 800 m appears both too thick and too resistive. In addition, the shallow EM data show some sensitivity to the interface at 2-m depth between frozen silty sands and frozen gravels, though the depth of this interface is over-estimated due to the limited sensitivity to these very resistive features.

4 Discussion

Understanding the hydrogeophysical responses to permafrost dynamics under different hydrologic and climatic conditions, and in different geological settings, is important for guiding the interpretation of existing geophysical datasets and also for planning future surveys. Geophysical models are inherently uncertain and ambiguous because of (1) the resolution limitations of any geophysical method and (2) the weak or non-unique relationship between hydrologic properties and geophysical properties. We have presented a general framework for coupling airborne and ground-based electromagnetic

Burke Minsley 2/24/2015 10:19 PM
Deleted: geophysical

predictions to hydrologic simulations of permafrost evolution, including a novel physical property relationship that accounts for the electrical response to changes in lithology, temperature, and ice content, as well as a rigorous analysis of geophysical parameter uncertainty. Although the focus here is on AEM data, other types of electrical or electromagnetic measurements could be readily simulated using the same resistivity model. Future efforts will focus on the simulation of other types of geophysical data (e.g. nuclear magnetic resonance or ground penetrating radar) using the same basic modeling approach.

In the specific examples of lake talik evolution presented here, which are modeled after the physical setting of the Yukon Flats, Alaska (Minsley et al., 2012b), AEM data are shown to be generally capable of resolving large-scale permafrost and geological features (Figure **5**), as well as thermally and hydrologically induced changes in permafrost (Figure **8**, Figure **9**). The Bayesian McMC analysis provides useful details about model resolution and uncertainty that cannot be assessed using traditional inversion methods that produce a single 'best' model. A fortuitous aspect of the Yukon Flats model is the fact that the silt layer (Unit 3) is relatively conductive compared with the overlying gravels (Unit 2), making it a good target for electromagnetic methods. If the order of these layers were reversed, if the base of permafrost were hosted in a relatively resistive lithology, or if the base of permafrost was significantly deeper, AEM data would not likely resolve the overall structure with such good fidelity. In addition, knowledge of the stratigraphy helps to remove the ambiguity between unfrozen gravels and frozen silts, which have similar intermediate resistivity values (Figure **4**, Figure **5**). The methods developed here that use a physical property model to link hydrologic and geophysical properties provide the necessary framework to test other more challenging hydrogeological scenarios.

Two key challenges for the lake talik scenarios were identified: (1) resolving the details of partial ice saturation beneath the lake during talik formation, and (2) resolving near-surface details associated with shallow thaw. The first challenge is confirmed by Figure **5** and Figure **8**, which show that AEM data cannot resolve the details of partial ice saturation beneath a forming talik. However, there is clearly a change in the overall characteristics of the sub-lake resistivity structure as thaw increases (Figure **9**). One

Burke Minsley 2/24/2015 10:22 PM
Deleted: over time

Burke Minsley 2/21/2015 3:44 PM
Deleted: or

notable feature is the steadily decreasing depth to the top of the low-resistivity unfrozen silt (red) beneath the lake (Figure **5**A-B) as thaw increases, ultimately terminating at the depth of the gravel-silt interface when fully unfrozen conditions exist (Figure **5**C). Measurements of the difference in elevation between the interpreted top of unfrozen silt and the base of nearby frozen gravels were used by Jepsen et al. (2013a) to classify whether or not fully thawed conditions existed beneath lakes in the Yukon Flats AEM survey described by Minsley et al. (2012a). The simulations presented here support use of this metric to distinguish full versus partial thaw beneath lakes. However, without the presence of a lithological boundary, the shallowing base of permafrost associated with talik development beneath lakes would be much more difficult to distinguish. Finally, it is important to note that resistivity is sensitive primarily to unfrozen water content, and that significant unfrozen water can remain in relatively warm permafrost that is near 0 C, particularly in fine-grained sediments. Resistivity-derived estimates of talik boundaries defined by water content may therefore differ from the thermal boundary defined at 0 C.

The second challenge, to resolve near-surface details associated with supra-permafrost thaw, is addressed in Figure **10**. For the scenarios considered here, AEM data can identify shallow thaw features, but have difficulty in discriminating their specific details. There are many combinations of resistivity and thickness that produce the same EM response; therefore, without additional information it is not possible to uniquely characterize both thaw depth and resistivity. Ground-based EM data show improved sensitivity to the shallow channels, and also limited sensitivity to the interface between resistive frozen gravels and frozen silty sands (Figure **5**). By restricting the possible values of resistivity and/or thickness for one or more layers based on prior assumptions, Dafflon et al. (2013) showed that improved estimates of active layer and permafrost properties can be obtained. The quality of these estimates, of course, depends on the accuracy of prior constraints used. In many instances, it may be possible to auger into this shallow layer to provide direct observations that can be used as constraints. This approach could be readily applied to the ensemble of McMC models. For example, if the resistivity of the channels in Figure **10**A were known, the thickness of the channels could be estimated more accurately by selecting only the set of McMC models with channel

resistivity close to the true value, thereby removing some of the ambiguity due to equivalences between layer resistivity and thickness.

AEM data are most likely to be useful for baseline characterization of subsurface properties as opposed to monitoring changes in permafrost. Although there are some cases of rapid change associated with near-surface freeze/thaw processes (Koch et al., 2013) or in the case of catastrophic loss of ice in the gaining lake scenario (Figure **9**B) that may be of interest, large-scale changes in permafrost generally occur over much longer time periods than is practical for repeat AEM surveys. One exception could be related to infrastructure projects such as water reservoirs or mine tailing impoundments behind dams, where AEM could be useful for baseline characterization and repeat monitoring of the impact caused by human-induced permafrost change. Geophysical modeling, thermophysical hydrologic modeling, and field observations create a synergy that provides greater insight than any individual approach, and can be useful for future characterization of coupled permafrost and hydrologic processes.

5 Summary

Analysis of AEM surveys provide a means for remotely detecting subsurface electrical resistivity associated with the co-evolution of permafrost and hydrologic systems over areas relevant to catchment-scale and larger processes. Coupled hydrogeophysical simulations using a novel physical property relationship that accounts for the effects of lithology, ice saturation, and temperature on electrical resistivity provide a systematic framework for exploring the geophysical response to various scenarios of permafrost evolution under different hydrological forcing. This modeling approach provides a means of robustly testing the interpretation of AEM data given the paucity of deep boreholes and other ground truth data that are needed to characterize subsurface permafrost. A robust uncertainty analysis of the geophysical simulations provides important new quantitative information about the types of features that can be resolved using AEM data given the inherent resolution limitations of geophysical measurements and ambiguities in the physical property relationships. In the scenarios considered here, we have shown that large-scale geologic and permafrost structure is accurately estimated. Sublacustrine thaw can also be identified, but the specific geometry of partial ice

Burke Minsley 2/23/2015 10:03 PM
Deleted: what

saturation beneath lakes can be poorly resolved by AEM data. Understanding the geophysical response to known simulations is helpful both for guiding the interpretation of existing AEM data, and also to plan future surveys and other ground-based data acquisition efforts.

Author contribution

B. M. carried out the geophysical forward and inverse simulations, and prepared the manuscript with contributions from all co-authors. T. W. and M. W. provided SUTRA simulation results and hydrologic modeling expertise. A. R. helped to establish the petrophysical relationships used to define the electrical resistivity model used in this study.

Acknowledgements

This work was supported by the Strategic Environmental Research and Development Program (SERDP), through grant #RC-2111. We gratefully acknowledge additional support from the USGS National Research Program and the USGS Geophysical Methods Development Project. USGS reviews provided by Josh Koch and Marty Briggs have greatly improved this manuscript.

References

Anthony, K. M. W., Anthony, P., Grosse, G. and Chanton, J.: Geologic methane seeps along boundaries of Arctic permafrost thaw and melting glaciers, Nat. Geosci., 5, 419–426, doi:10.1038/ngeo1480, 2012.

Archie, G. E.: The electrical resistivity log as an aid in determining some reservoir characteristics, Trans Amer Inst Min. Metall. Pet. Eng., 146, 54–62, 1942.

Aster, R. C., Borchers, B. and Thurber, C. H.: Parameter Estimation and Inverse Problems, Elsevier, Amsterdam., 2005.

Ball, L. B., Smith, B. D., Minsley, B. J., Abraham, J. D., Voss, C. I., Deszcz-Pan, M. and Cannia, J. C.: Airborne electromagnetic and magnetic survey data of the Yukon Flats and Ft. Wainwright areas, central Alaska, June 2010, U.S. Geological Survey Open-File Report 2011-1304., 2011.

Beamish, D.: Airborne EM footprints, Geophys. Prospect., 51(1), 49–60, doi:10.1046/j.1365-2478.2003.00353.x, 2003.

Bense, V. F., Ferguson, G. and Kooi, H.: Evolution of shallow groundwater flow systems in areas of degrading permafrost, Geophys. Res. Lett., 36, L22401, doi:200910.1029/2009GL039225, 2009.

Briggs, M. A., Walvoord, M. A., McKenzie, J. M., Voss, C. I., Day-Lewis, F. D. and Lane, J. W.: New permafrost is forming around shrinking Arctic lakes, but will it last?, Geophys. Res. Lett., 41(5), 2014GL059251, doi:10.1002/2014GL059251, 2014.

Callegary, J. B., Kikuchi, C. P., Koch, J. C., Lilly, M. R. and Leake, S. A.: Review: Groundwater in Alaska (USA), Hydrogeol. J., 21(1), 25–39, doi:10.1007/s10040-012-0940-5, 2013.

Dafflon, B., Hubbard, S. S., Ulrich, C. and Peterson, J. E.: Electrical Conductivity Imaging of Active Layer and Permafrost in an Arctic Ecosystem, through Advanced Inversion of Electromagnetic Induction Data, Vadose Zone J., 12(4), vzj2012.0161, doi:10.2136/vzj2012.0161, 2013.

Day-Lewis, F. D., Singha, K. and Binley, A. M.: Applying petrophysical models to radar travel time and electrical resistivity tomograms: Resolution-dependent limitations, J. Geophys. Res. Solid Earth, 110, B08206, doi:10.1029/2004JB003569, 2005.

Farquharson, C. G., Oldenburg, D. W. and Routh, P. S.: Simultaneous 1D inversion of loop–loop electromagnetic data for magnetic susceptibility and electrical conductivity, Geophysics, 68(6), 1857–1869, doi:10.1190/1.1635038, 2003.

Green, P. J.: Reversible jump Markov chain Monte Carlo computation and Bayesian model determination, Biometrika, 82(4), 711–732, 1995.

Burke Minsley 2/24/2015 10:02 PM
Formatted: Bibliography, Widow/Orphan control, Adjust space between Latin and Asian text, Adjust space between Asian text and numbers

Burke Minsley 2/24/2015 10:01 PM
Deleted: Anthony, K. M. W., Anthony, P., Grosse, G. and Chanton, J.: Geologic methane seeps along boundaries of Arctic permafrost thaw and melting glaciers, Nat. Geosci., 5, 419–426, doi:10.1038/ngeo1480, 20 ... [1]

Hastings, W. K.: Monte Carlo sampling methods using Markov chains and their applications, Biometrika, 57(1), 97–109, doi:10.1093/biomet/57.1.97, 1970.

Hauck, C., Böttcher, M. and Maurer, H.: A new model for estimating subsurface ice content based on combined electrical and seismic data sets, The Cryosphere, 5(2), 453–468, doi:10.5194/tc-5-453-2011, 2011.

Hinzman, L. D., Bettez, N. D., Bolton, W. R., Chapin, F. S., Dyurgerov, M. B., Fastie, C. L., Griffith, B., Hollister, R. D., Hope, A., Huntington, H. P., Jensen, A. M., Jia, G. J., Jorgenson, T., Kane, D. L., Klein, D. R., Kofinas, G., Lynch, A. H., Lloyd, A. H., McGuire, A. D., Nelson, F. E., Oechel, W. C., Osterkamp, T. E., Racine, C. H., Romanovsky, V. E., Stone, R. S., Stow, D. A., Sturm, M., Tweedie, C. E., Vourlitis, G. L., Walker, M. D., Walker, D. A., Webber, P. J., Welker, J. M., Winker, K. S. and Yoshikawa, K.: Evidence and implications of recent climate change in northern Alaska and other Arctic regions, Clim. Change, 72(3), 251–298, doi:10.1007/s10584-005-5352-2, 2005.

Hoekstra, P., Sellmann, P. V. and Delaney, A.: Ground and airborne resistivity surveys of permafrost near Fairbanks, Alaska, Geophysics, 40(4), 641–656, 1975.

Huang, H. P. and Won, I. J.: Real-time resistivity sounding using a hand-held broadband electromagnetic sensor, Geophysics, 68(4), 1224–1231, 2003.

Hubbard, S. S., Gangodagamage, C., Dafflon, B., Wainwright, H., Peterson, J., Gusmeroli, A., Ulrich, C., Wu, Y., Wilson, C., Rowland, J., Tweedie, C. and Wullschleger, S. D.: Quantifying and relating land-surface and subsurface variability in permafrost environments using LiDAR and surface geophysical datasets, Hydrogeol. J., 21(1), 149–169, doi:10.1007/s10040-012-0939-y, 2013.

Jepsen, S. M., Voss, C. I., Walvoord, M. A., Minsley, B. J. and Rover, J.: Linkages between lake shrinkage/expansion and sublacustrine permafrost distribution determined from remote sensing of interior Alaska, USA, Geophys. Res. Lett., 40(5), 882–887, doi:10.1002/grl.50187, 2013a.

Jepsen, S. M., Voss, C. I., Walvoord, M. A., Rose, J. R., Minsley, B. J. and Smith, B. D.: Sensitivity analysis of lake mass balance in discontinuous permafrost: the example of disappearing Twelvemile Lake, Yukon Flats, Alaska (USA), Hydrogeol. J., 21(1), 185–200, doi:10.1007/s10040-012-0896-5, 2013b.

Jorgenson, M. T., Racine, C., Walters, J. and Osterkamp, T.: Permafrost degradation and ecological changes associated with a warming climate in central Alaska, Clim. Change, 48(4), 551–579, 2001.

Keller, G. V. and Frischknecht, F. C.: Electrical methods in geophysical prospecting, Pergamon Press, Oxford., 1966.

Koch, J. C., Ewing, S. A., Striegl, R. and McKnight, D. M.: Rapid runoff via shallow throughflow and deeper preferential flow in a boreal catchment underlain by frozen

silt (Alaska, USA), Hydrogeol. J., 21(1), 93–106, doi:10.1007/s10040-012-0934-3, 2013.

Koven, C. D., Ringeval, B., Friedlingstein, P., Ciais, P., Cadule, P., Khvorostyanov, D., Krinner, G. and Tarnocai, C.: Permafrost carbon-climate feedbacks accelerate global warming, Proc. Natl. Acad. Sci., 108(36), 14769 –14774, doi:10.1073/pnas.1103910108, 2011.

Larsen, P. H., Goldsmith, S., Smith, O., Wilson, M. L., Strzepek, K., Chinowsky, P. and Saylor, B.: Estimating future costs for Alaska public infrastructure at risk from climate change, Glob. Environ. Gov. Another World Possible, 18(3), 442–457, doi:10.1016/j.gloenvcha.2008.03.005, 2008.

Liu, L., Schaefer, K., Zhang, T. and Wahr, J.: Estimating 1992–2000 average active layer thickness on the Alaskan North Slope from remotely sensed surface subsidence, J. Geophys. Res. Earth Surf., 117, F01005, doi:10.1029/2011JF002041, 2012.

Marion, G. M.: Freeze-thaw processes and soil chemistry., 1995.

McKenzie, J. and Voss, C.: Permafrost thaw in a nested groundwater-flow system, Hydrogeol. J., 21(1), 299–316, doi:10.1007/s10040-012-0942-3, 2013.

Metropolis, N., Rosenbluth, A., Rosenbluth, M., Teller, A. and Teller, E.: Equation of State Calculations by Fast Computing Machines, J. Chem. Phys., 21(6), 1087–1092, doi:10.1063/1.1699114, 1953.

Minsley, B. J.: A trans-dimensional Bayesian Markov chain Monte Carlo algorithm for model assessment using frequency-domain electromagnetic data, Geophys. J. Int., 187(1), 252–272, doi:10.1111/j.1365-246X.2011.05165.x, 2011.

Minsley, B. J., Abraham, J. D., Smith, B. D., Cannia, J. C., Voss, C. I., Jorgenson, M. T., Walvoord, M. A., Wylie, B. K., Anderson, L., Ball, L. B., Deszcz-Pan, M., Wellman, T. P. and Ager, T. A.: Airborne electromagnetic imaging of discontinuous permafrost, Geophys. Res. Lett., 39, L02503, doi:10.1029/2011GL050079, 2012a.

Minsley, B. J., Abraham, J. D., Smith, B. D., Cannia, J. C., Voss, C. I., Jorgenson, M. T., Walvoord, M. A., Wylie, B. K., Anderson, L., Ball, L. B., Deszcz-Pan, M., Wellman, T. P. and Ager, T. A.: Airborne electromagnetic imaging of discontinuous permafrost, Geophys. Res. Lett., 39, L02503, doi:10.1029/2011GL050079, 2012b.

Minsley, B. J., Ajo-Franklin, J., Mukhopadhyay, A. and Morgan, F. D.: Hydrogeophysical Methods for Analyzing Aquifer Storage and Recovery Systems, Ground Water, 49(2), 250–269, 2011.

Nelson, F. E., Anisimov, O. A. and Shiklomanov, N. I.: Climate change and hazard zonation in the crcum-Arctic permafrost regions, Nat. Hazards, 26(3), 203–225, 2002.

O'Donnell, J. A., Aiken, G. R., Walvoord, M. A. and Butler, K. D.: Dissolved organic matter composition of winter flow in the Yukon River basin: Implications of permafrost thaw and increased groundwater discharge, Glob. Biogeochem. Cycles, 26(4), GB0E06, doi:10.1029/2012GB004341, 2012.

O'Donnell, J. A., Harden, J. W., McGuire, A. D., Kanevskiy, M. Z., Jorgenson, M. T. and Xu, X.: The effect of fire and permafrost interactions on soil carbon accumulation in an upland black spruce ecosystem of interior Alaska: implications for post-thaw carbon loss, Glob. Change Biol., 17(3), 1461–1474, doi:10.1111/j.1365-2486.2010.02358.x, 2011.

Oldenborger, G. A. and Routh, P. S.: The point-spread function measure of resolution for the 3-D electrical resistivity experiment, Geophys. J. Int., 176(2), 405–414, 2009.

Palacky, G. J.: Resistivity characteristics of geologic targets, in Electromagnetic methods in applied geophysics: Voume 1, theory, edited by M. N. Nabighian, pp. 53–129, Society of Exploration Geophysicists, Tulsa., 1987.

Panda, S. K., Prakash, A., Solie, D. N., Romanovsky, V. E. and Jorgenson, M. T.: Remote sensing and field-based mapping of permafrost distribution along the Alaska Highway corridor, interior Alaska, Permafr. Periglac. Process., 21(3), 271–281, doi:10.1002/ppp.686, 2010.

Parsekian, A. D., Grosse, G., Walbrecker, J. O., Müller-Petke, M., Keating, K., Liu, L., Jones, B. M. and Knight, R.: Detecting unfrozen sediments below thermokarst lakes with surface nuclear magnetic resonance, Geophys. Res. Lett., 40(3), 535–540, doi:10.1002/grl.50137, 2013.

Pastick, N. J., Jorgenson, M. T., Wylie, B. K., Rose, J. R., Rigge, M. and Walvoord, M. A.: Spatial variability and landscape controls of near-surface permafrost within the Alaskan Yukon River Basin, J. Geophys. Res. Biogeosciences, 119(6), 2013JG002594, doi:10.1002/2013JG002594, 2014.

Petrone, K. C., Hinzman, L. D., Jones, J., Shibata, H. and Boone, R.: The influence of fire and permafrost on sub-arctic stream chemistry during storms, Hydrol. Process., 21(4), 423–434, doi:10.1002/hyp.6247, 2007.

Revil, A.: Spectral induced polarization of shaly sands: Influence of the electrical double layer, Water Resour. Res., 48(W02517), doi:10.1029/2011WR011260, 2012.

Revil, A., Cathles, L. M., Losh, S. and Nunn, J. A.: Electrical conductivity in shaly sands with geophysical applications, J. Geophys. Res. Solid Earth, 103(B10), 23925–23936, doi:10.1029/98JB02125, 1998.

Rinaldi, A. P., Todesco, M., Vandemeulebrouck, J., Revil, A. and Bonafede, M.: Electrical conductivity, ground displacement, gravity changes, and gas flow at Solfatara crater (Campi Flegrei caldera, Italy): Results from numerical modeling, J. Volcanol. Geotherm. Res., 207(3–4), 93–105, doi:10.1016/j.jvolgeores.2011.07.008, 2011.

Roach, J., Griffith, B., Verbyla, B. and Jones, J.: Mechanisms influencing changes in lake area in Alaskan boreal forest, Glob. Change Biol., 17, 2567–2583, doi:10.1111/j.1365-2486.2011.02446.x, 2011.

Rover, J., Ji, L., Wylie, B. K. and Tieszen, L. L.: Establishing water body areal extent trends in interior Alaska from multi-temporal Landsat data, Remote Sens. Lett., 3(7), 595–604, doi:10.1080/01431161.2011.643507, 2012.

Rowland, J. C., Travis, B. J. and Wilson, C. J.: The role of advective heat transport in talik development beneath lakes and ponds in discontinuous permafrost, Geophys. Res. Lett., 38, L17504, doi:10.1029/2011GL048497, 2011.

Sambridge, M., Bodin, T., Gallagher, K. and Tkalčić, H.: Transdimensional inference in the geosciences, Philos. Trans. R. Soc. Math. Phys. Eng. Sci., 371(1984), doi:10.1098/rsta.2011.0547, 2013.

Sen, P. N. and Goode, P. A.: Influence of temperature on electrical conductivity on shaly sands, Geophysics, 57(1), 89–96, doi:10.1190/1.1443191, 1992.

Sen, P., Scala, C. and Cohen, M.: A self‐similar model for sedimentary rocks with application to the dielectric constant of fused glass beads, Geophysics, 46(5), 781–795, doi:10.1190/1.1441215, 1981.

Siemon, B.: Electromagnetic methods - frequency domain, in Groundwater Geophysics: A Tool for Hydrogeology, edited by R. Kirsch, pp. 155–176, Springer-Verlag, Berlin., 2006.

Striegl, R. G., Aiken, G. R., Dornblaser, M. M., Raymond, P. A. and Wickland, K. P.: A decrease in discharge-normalized DOC export by the Yukon River during summer through autumn, Geophys. Res. Lett., 32, L21413, doi:10.1190/1.1443191, 2005.

Voss, C. I. and Provost, A. M.: SUTRA, A model for saturated-unsaturated, variable density ground-water flow with solute or energy transport, U.S. Geological Survey Water-Resources Investigations Report 02-4231., 2002.

Walvoord, M. A. and Striegl, R. G.: Increased groundwater to stream discharge from permafrost thawing in the Yukon River basin: Potential impacts on lateral export of carbon and nitrogen, Geophys. Res. Lett., 34, L12402, doi:200710.1029/2007GL030216, 2007.

Walvoord, M. A., Voss, C. I. and Wellman, T. P.: Influence of permafrost distribution on groundwater flow in the context of climate-driven permafrost thaw: Example from Yukon Flats Basin, Alaska, United States, Water Resour. Res., 48(7), W07524, doi:10.1029/2011WR011595, 2012.

Ward, S. H. and Hohmann, G. W.: Electromagnetic theory for geophysical applications, in Electromagnetic methods in applied geophysics: Volume 1, theory, edited by M. N. Nabighian, pp. 131–311, Society of Exploration Geophysicists, Tulsa., 1988.

Wellman, T. P., Voss, C. I. and Walvoord, M. A.: Impacts of climate, lake size, and supra- and sub-permafrost groundwater flow on lake-talik evolution, Yukon Flats, Alaska (USA), Hydrogeol. J., 21(1), 281–298, doi:10.1007/s10040-012-0941-4, 2013.

Williams, J. R.: Geologic reconnaissance of the Yukon Flats District Alaska, U.S. Geological Survey Bulletin 1111-H., 1962.

Yoshikawa, K., Bolton, W. R., Romanovsky, V. E., Fukuda, M. and Hinzman, L. D.: Impacts of wildfire on the permafrost in the boreal forests of Interior Alaska, J. Geophys. Res. Atmospheres, 107(8148), doi:10.1029/2001JD000438, 2002.

Tables

Table 1. Description of geologic units and physical properties used in numerical simulations. Entries separated by commas represent parameters with different values for each of the lithologic units.

Geologic unit properties	
Lithology:	
Unit 1	Sediment (silty sand)
Unit 2	Sediment (gravelly sand)
Unit 3	Lacustrine silt
Unit depth range [m]	0-2, 2-30, 30-250
Porosity [-]	0.25, 0.25, 0.20
Geophysical parameters	
Archie cementation exponent (m) [-]	1.5
Archie saturation exponent (n) [-]	1.5
Water salinity (C) [ppm]	250 ($S_i = 0$)
Na^+ ionic mobility (β) [m^2/Vs]	5.8 x 10^{-8} (25°C)
Cl^- ionic mobility (β) [m^2/Vs]	7.9 x 10^{-8} (25°C)
Na^+ surface ionic mobility (β_s) [m^2/Vs]	0.51 x 10^{-8} (25°C)
Grain mass density (ρ_g) [kg/m^3]	2650
Cation exchange capacity (χ) [C/kg]	200, 10, 500
Salinity exponent (a) [-]	0.8

1422 Table 2. Probability of ice saturation falling above or below specified thresholds based
1423 on the McMC-derived resistivity probability distributions shown in Figure 7.

	p(ice < 0.5)	**p(ice > 0.95)**
Unit 2 (gravel), *r* = 0 m	0.76	0.05
Unit 2 (gravel), *r* = 750 m	0.00	0.88
Unit 3 (silt), *r* = 0 m	0.76	0.05
Unit 3 (silt), *r* = 750 m	0.00	0.98

1424

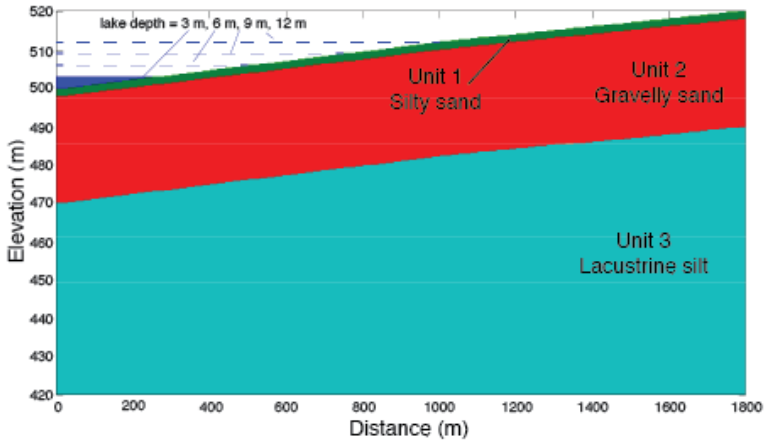

Figure 1. Axis-symmetric model geometry indicating different lithologic units and simulated lake depths/extents.

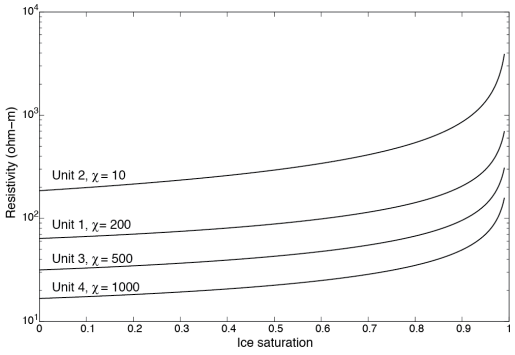

1430

1431 Figure 2. Bulk resistivity as a function of ice saturation using the physical properties
1432 defined for each of the lithologic units described in Table 1.

1433

1434

1435

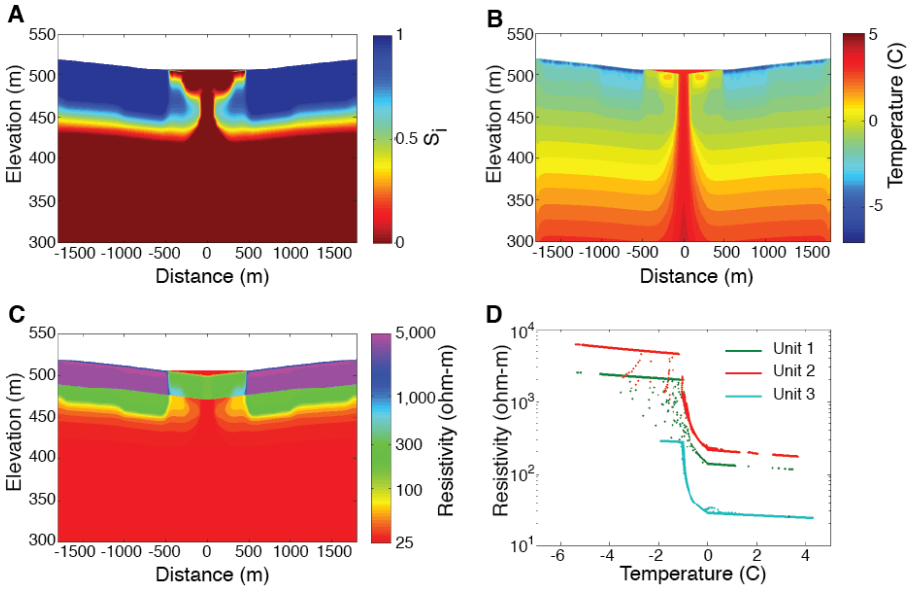

1436

1437 Figure 3. SUTRA model outputs and geophysical transformations from the 6-m gaining
1438 lake simulation at 240 years. Ice saturation (A) and temperature (B) are converted to
1439 predictions of bulk resistivity (C). Variability in resistivity as a function of temperature
1440 is indicated in (D) for lithologic units 1-3.

1441

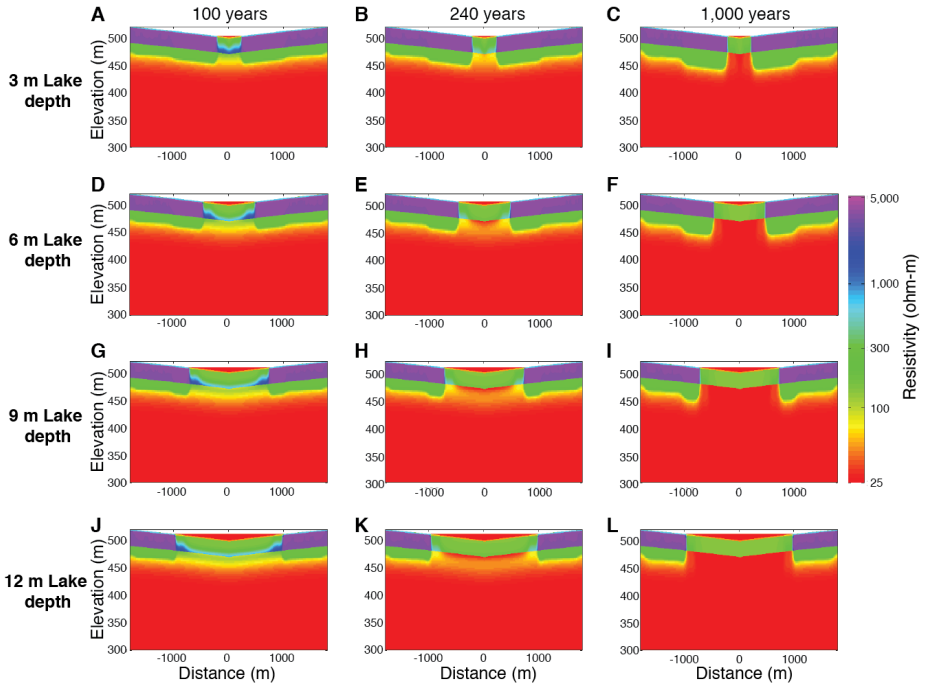

1442

1443 Figure 4. Synthetic bulk resistivity images under hydrostatic flow and current climate
1444 conditions. Lake depths of 3 m (A-C), 6 m (D-F), 9 m (G-I), and 12 m (J-L) are
1445 illustrated at simulation times 100, 240, and 1,000 years.

1446

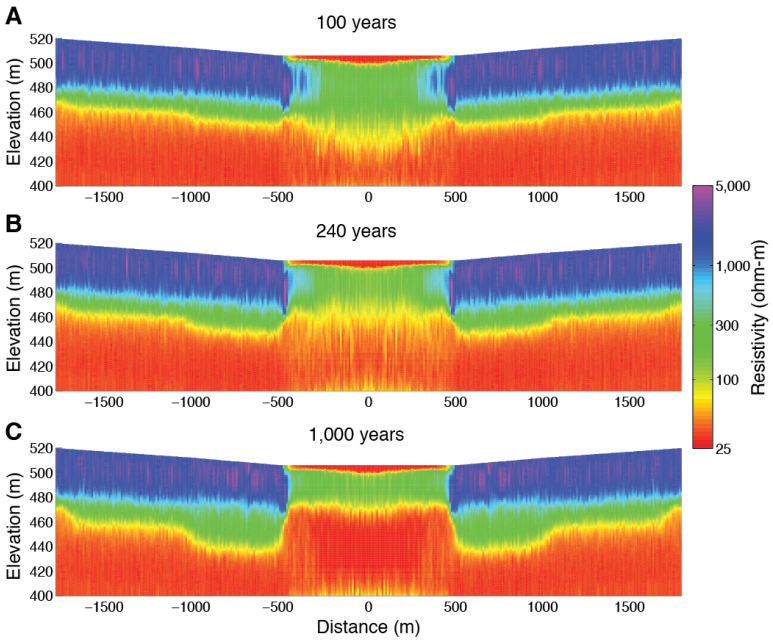

1447

1448 Figure 5. Mean resistivity model extracted from McMC ensembles. Results are shown
1449 for the 6-m-deep hydrostatic lake scenario outputs at (A) 100 years, (B) 240 years, and
1450 (C) 1,000 years.

1451

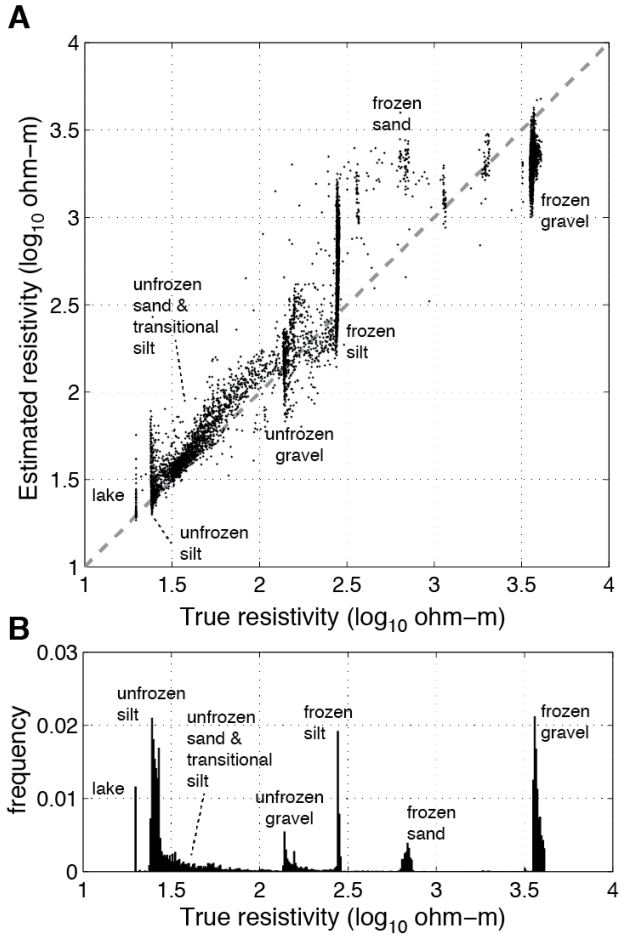

Figure 6. Performance of geophysical parameter estimation in recovering true parameter values. (A) True versus McMC-estimated resistivity values for the hydrostatic 6-m-deep lake scenario at simulation time 1,000 years, compared with the frequency distribution of true resistivity values (B). Estimated resistivity values generally fall along the dashed 1:1 line in (A), with exceptions being under-prediction of the resistive frozen gravels, over-prediction of the thin surficial frozen sand, and some over-prediction of the frozen silt where it is in contact with frozen gravel.

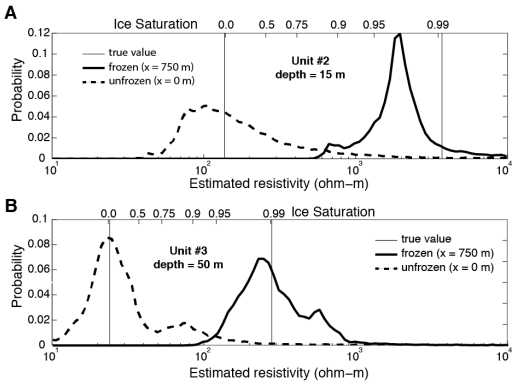

1461

1462 Figure 7. McMC-estimated resistivity posterior distributions within frozen and unfrozen
1463 unit #2 gravels (A) and frozen and unfrozen unit #3 silts (B) for the hydrostatic 6-m-deep
1464 lake scenario at 1,000 years. Unfrozen resistivity distributions are extracted beneath the
1465 center of the lake ($r = 0$) at depths of 15 m and 50 m for the gravels and silts,
1466 respectively. Frozen distributions are extracted at the same depths, but at $r = 750$ m. The
1467 upper x-axes labels indicate approximate ice saturation based on the lithology-dependent
1468 ice saturation versus resistivity curves shown in Figure 2.

1469

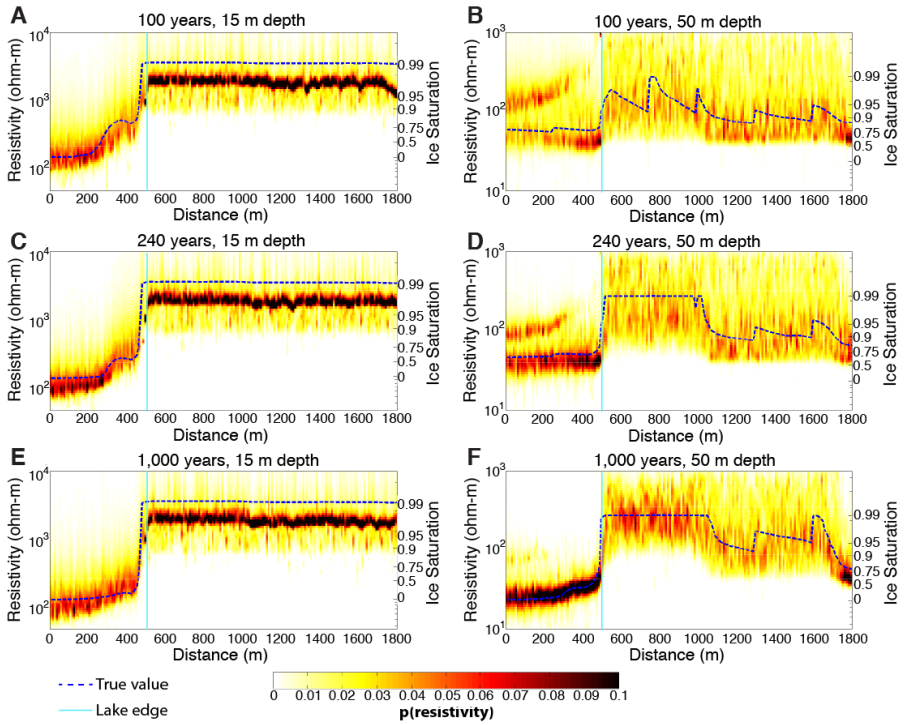

1470

1471 Figure 8. Resistivity probability distributions for the hydrostatic 6-m-deep lake scenario
1472 at simulation times 100 years (A-B), 240 years (C-D), and 1,000 years (E-F). Shading in
1473 each image represents the probability distribution at depths of 15 m (A, C, E) and 50 m
1474 (B, D, F) from the lake center (r = 0 m) to the edge of the model (r = 1800 m). Dashed
1475 lines indicate the true resistivity values. Ice saturation is displayed on the right axis of
1476 each image, and is defined empirically for each lithology using the relationships in Figure
1477 2.

1478

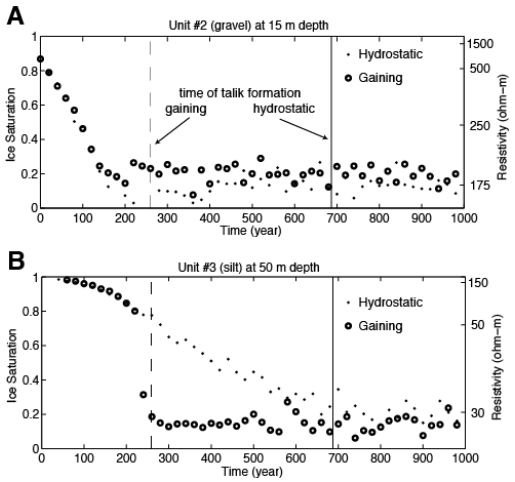

Figure 9. Change in ice saturation and resistivity as a function of time. Results are shown for the 6-m-deep lake hydrostatic and gaining lake scenarios within (A) the gravel layer, unit #2, at a depth of 15 m and (B) the silt layer, unit #3, at a depth of 50 m.

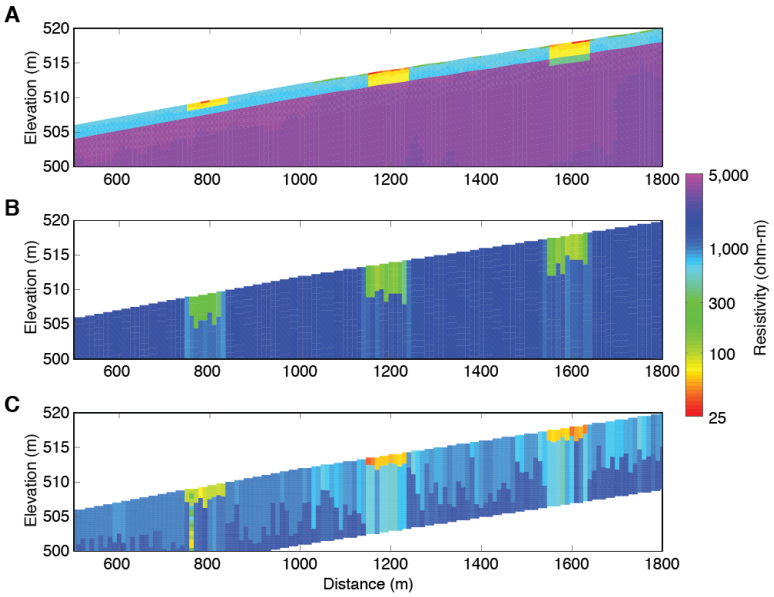

Figure 10. Comparison of airborne and ground-based measurements for recovering shallow thaw features. (A) True shallow resistivity structure extracted from the hydrostatic 6-m-deep lake scenario at a simulation time of 1,000 years, shown outside of the lake extent (distance > 500 m). Three shallow low-resistivity channels with thicknesses 1 m, 2 m, and 3 m were added to the resistivity model to provide added contrast. McMC-derived results using simulated AEM data (B) and ground-based EM data (C) illustrate the capability of these systems to image shallow features.